IJISET - International Journal of Innovative Science, Engineering & Technology, Vol. 3 Issue 10, October 2016
ISSN (Online) 2348 – 7968 | Impact Factor (2015) - 4.332
www.ijiset.com

Structural, morphological, compositional and infra-red properties of $NiAl_{2x}Cr_xFe_{2-3x}O_4$ ($0.0 \leq x \leq 0.2$) nanoparticles

Shridhar K. Hukkeri[1*], Shankar D. Birajdar[2], R. G. Kulkarni[1], Shrikant Ekhelikar[3], K. M. Jadhav[2]

[1]Department of Physics, G.S.S. College, Belgaum, India
[2]Department of physics, Dr. Babasaheb Ambedkar Marathwada University, Aurangabad, India
[3]Department of Physics, N.V. College, Gulbarga, India
shreehukkeri@gmail.com

Abstract

A series of $NiAl_{2x}Cr_xFe_{2-3x}O_4$ (x = 0.0, 0.1 and, 0.2) spinel ferrites nanoparticles were synthesized by sol-gel auto combustion method. The samples were characterized by X-ray diffraction (XRD), scanning electron microscopy (SEM), and energy dispersive X-ray analysis (EDAX) and Fourier transform infrared spectroscopy (FT-IR). The X-ray diffraction analysis revealed the formation of single phase having spinel cubic structure. Lattice parameter, X-ray density, bulk density and particle size decrease with the increase in Al-Cr content 'x'. SEM analysis clearly showed the small agglomeration present in the nanoparticles. The average grain size obtained from scanning electron microscopy was found in the range of 76-87 nm. Energy dispersive spectroscopy analysis confirmed that the synthesized samples were near stoichiometric. The FTIR studies show two absorption bands at about 400 cm^{-1} and 600 cm^{-1} for octahedral and tetrahedral sites respectively.

Keywords: *XRD; SEM; Nanoparticles; FTIR.*

1. Introduction

Spinel ferrites have been extensively investigated in the past two decades for their useful electrical and magnetic properties [1-4]. They have different applications in information storage systems, magnetic cores, magnetic fluids, electronic devices, microwave absorbers, sensors, magnetic drug delivery, and medical diagnostics [5, 6]. Among the various type of ferrites materials, nickel ferrite shows ferrimagnetism that originates from a magnetic moment of anti-parallel spins between Fe^{3+} ions at tetrahedral and octahedral sites and Ni^{2+} ions at octahedral sites [7]. Nickel ferrite is a technologically important material, used in a wide variety of applications, including computer components, antenna rods, transformer cores, satellite communications and memory devices [8]. Apart from this, these materials are also used extensively as isolators, circulators and phase shifters etc., at microwave frequencies [9]. This could be due to their interesting properties like, (i) high resistivity 10^6 Ω cm, and hence lower eddy current losses, (ii) low dielectric and magnetic losses, (iii) high saturation magnetization 50 emu/g, (iv) low-cost of fabrication and (v) high Curie temperature (853 K). Nickel ferrite ($NiFe_2O_4$) has an inverse spinel structure. In this structure Ni^{2+} ions occupy octahedron B sites and Fe^{3+} ions occupy both the tetrahedron (A) and the octahedron [B] sites. In a spinel structure there are 56 ions, 32 oxygen ions and 24 metal ions in a unit cell. In this structure eight molecules occupy one unit cell of the spinel. A general formula for a ferrite structure is $(M_{1-x}Fe_x)[M_xFe_{2-x}]\ O_4$, where M stands for cations which occupy tetrahedron sites and x is the degree of inversion [10, 11]. Many works concerning the synthesis and magnetic properties of nickel ferrite have been published [12, 13]. Recently, the diamagnetic ion substitutions in spinel ferrites have received special attention. It has been reported earlier that in spinel ferrites, if Fe ions are replaced by Al $^{3+}$, In $^{3+}$, Cr $^{3+}$, Gd $^{3+}$, RE $^{3+}$, and Ti $^{4+}$ [14, 15].

In the literature, reports are available for the synthesis and characterization of nickel ferrite substituted with various cations separately like Al, Cr, Co, Mn etc., [16]. Magalhaes et al. [17] synthesized a series of ferrite samples with compositions $Fe_{3-x}Cr_xO4$ (x = 0.00, 0.07, 0.26, 0.42, and 0.51) by the conventional co-precipitation method. They considered that Cr^{3+} ions replaced Fe^{3+} ions at the [B] sites at low Cr content, and then with increasing Cr content, the chromium ions substituted for Fe^{2+} ions at the [B] sites and Fe^{3+} ions at the (A) sites. Ghatage et al., [18] prepared $NiCr_xFe_{2-x}O_4$ ($0.2 \leq x \leq 1.0$, in steps of 0.2) via the usual ceramic method. Using neutron diffraction, they concluded that the number of Cr ions per formula at the (A) sites increased from 0.10 to 0.30 as x increased from 0.2 to 1.0. In Al-containing ferrites, Al ions exists in the tetrahedral (A) and octahedral [B] sites depending on the amount of Al in the ferrite and then it well change the amount of the iron ions in the two sites. The bulk material in ferrites is assumed to be constituted of highly conduction grains separated by low conducting grain boundaries, this heterogeneous structure of ferrites may greatly affect the dielectric properties of the material [19]. A. T. Raghavender et al. [20] have studied the synthesis and magnetic properties of $NiFe_{2-x}Al_xO_4$ nanoparticles.

In the literature, reports are available for the synthesis and characterization of nickel ferrite substituted with various cations separately like Al^{3+}, Cr^{3+}. These studies revealed that the structural, electrical and magnetic properties of nickel ferrite are strongly influenced with the substitution of multivalent cations. In particular, the co-substitution of Cr^{3+} and Al^{3+} ions at the Fe^{3+} site are known to produce very interesting physical and chemical properties in spinel ferrites. The substitution of Al^{3+} and Cr^{3+} ions in the crystal structure of nickel ferrite can significantly affect on structural and magnetic properties by changing the magneto-crystalline anisotropy field. Here, by replacing the Fe^{3+} ions by Al^{3+} and Cr^{3+} ions [21], we expected to obtain the nickel ferrite that possess high anisotropy field. Also, the electrical and dielectric properties are expected to be significantly changed. Thus, it will be interesting to study the structural, micro structural, electrical and magnetic properties of Al^{3+} and Cr^{3+} ions co-substituted nickel ferrite nanoparticles. The investigations of structural, morphological, electrical and magnetic properties of Al^{3+} and Cr^{3+} ions doped in nickel ferrite nanoparticles are important from the point of view of its use in electrical and electronic applications.

To our knowledge, the effect of co-substitution of Al^{3+} and Cr^{3+}ions in nickel ferrite on the structural, morphological, infra-red properties has not been reported in the literature. In view of the above facts, the aim of the present work is to investigate the structural, morphological, infrared properties of $NiAl_{2x}Cr_xFe_{2-3x}O_4$ nanoparticles **(**x = 0.0, 0.1, 0.2) as a function of Al^{3+} and Cr^{3+} co-content x and to find correlation between the various properties.

2. Experimental

2.1 Synthesis of $NiAl_{2x}Cr_xFe_{2-3x}O_4$ nanoparticles

Analytical Reagent (AR) grade nickel nitrate Ni $(NO_3)_2.6H_2O$, ferric nitrate $Fe(NO_3)_3.9H_2O$, aluminum nitrate Al $(NO_3)_3.9H_2O$, chromium nitrate $Cr(NO_3)_3.9H_2O$ and citric acid $C_6H_8O_7.H_2O$ as a fuel were used as starting materials. According to the composition of $NiAl_{2x}Cr_xFe_{2-3x}O_4$ **(**where x = 0.0, 0.1, 0.2), all the nitrates were separately dissolved in minimum amount of distilled water and stirred on magnetic stirrer for ten minutes. All the solutions were mixed together and stirred on a magnetic stirrer until the nitrates were completely dissolved. The metal nitrate to citric acid ratio was taken as 1:3. The solutions were stirred with continuous stirring on magnetic stirrer; drop by drop ammonia solution was added to adjust the pH value to 7. Then the solution was heated on hot plate at 90˚C with constant stirring until gel was formed. Instantaneously gel ignites with the formation of large amount of gas, resulting in to light weight voluminous powder. The resulting precursor powder was annealed at 800˚C for 12 h to obtain $NiAl_{2x}Cr_xFe_{2-3x}O_4$ nano-powder.

2.2 Characterizations

The powder X-ray diffraction (XRD) pattern for all the samples were recorded at room temperature on Philips X-ray diffractometer (Model 3710) using Cu-Kα radiation (λ = 1.5406 Å).The surface morphological studies were carried out using SEM using JEOL-JSM-5600. The stoichiometric proportion of the constituent of the prepared magnetic nano-particles was examined using energy dispersive analysis of X-ray (EDAX) technique with the help of JEOL-JSM-5600 scanning electron micrograph (SEM). The Fourier transform infrared spectroscopy (FTIR) spectra of all the calcined samples were recorded in the range of 1000-300 cm^{-1} IR-BRUKER-TENSOR 37-FTIR-ATR instrument. The FTIR spectrum is generally used to investigate the chemical and structural changes that take place during the combustion process and to reveal the mechanism of self-propagating combustion.

3. Results and Discussion

Structural Properties

3.1 X-ray diffraction

X-ray diffraction pattern for typical x = 0.1 concentration is shown in Fig. 1.1. XRD analysis revealed that all the diffraction peaks seen in the XRD pattern well matches [22] with the standard pattern of pure nickel ferrite (JCPDS No: 10-325). The analysis of XRD pattern revealed the formation of single phase cubic spinel structure [23]. The intensity of (311) plane is more as compared to other planes like (220), (222), (400), (422), (511) and (440).

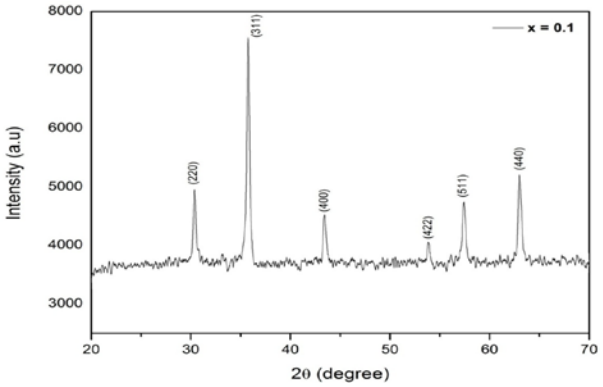

Fig.1.1: Typical XRD pattern of $NiAl_{2x}Cr_xFe_{2-3x}O_4$ nanoparticles for x = 0.1

The Lattice constant (a) values of the Al-Cr doped in nickel ferrite samples were calculated using standard relation [24].

$$a = d\sqrt{(h^2+k^2+l^2)} \quad Å \qquad (1)$$

where, (d) is interplanar spacing; (h k l) is Miller Indices.

The obtained values of the lattice constant (a) are tabulated in Table 1.1. It can be seen from Table 1.1 that lattice parameter goes on decreasing with increasing Al-Cr content *x*, this behavior of lattice constant with Al-Cr content *x* is explained on the basis of difference in ionic radii of constituent ions. The decrease of 'a' with *x* is because of the fact that the larger ionic radii of Fe^{3+} (0.67 Å) are replaced by smaller ionic radii of Al^{3+} (0.51 Å) and Cr^{3+} (0.63 Å) simultaneously. Our results are in good agreement with literature report for ceramic method [25].

Table 1.1 Lattice constant (a), X-ray density (d_x), bulk density (d_b), volume (V) and crystallite size (t) $NiAl_{2x}Cr_xFe_{2-3x}O_4$ ($0.0 \le x \le 0.2$) nanoparticles

x	a (Å)	d_x gm/cm^3	d_b gm/cm^3	V (Å)^3	t (nm)
0.0	8.3122	5.4203	4.733	574.3	38.44
0.1	8.3042	5.2931	4.698	572.7	30.00
0.2	8.2914	5.1742	4.681	570.0	28.49

The unit cell volume (V) was calculated by using the following equation [26]

$$V = a^3 \quad Å \qquad (2)$$

Where, V is the unit cell volume, 'a' is the lattice constant.

The unit cell volume (V) shows gradual decrease with the substitution of Al-Cr for ferrous in the present ferrite system. The decrease in cell volume is attributed to decrease in lattice constant of the system under investigation.

The X-ray density (d_x) [27] was calculated by using the relation and values are summarized in **Table 1.1**;

$$d_x = \frac{Z \times M}{V \times N_A} \qquad (3)$$

where, Z is the number of molecules per formula unit (Z = 8 for spinel system), M is molecular mass of the sample, $V = a^3$ is the unit cell volume, N_A is the Avogadro's number. It is observed from Table 1.1 that X-ray density decreases with increasing Al-Cr content *x*. This behavior of X-ray density is attributed to a decrease in mass that overtakes the decrease in volume of unit cell. The variation of X-ray density increases with the increase in Al-Cr content 'x'.

The bulk density of the present sample was obtained through Archimedes principle using toluene as an immersion liquid. The values of bulk density are reported in Table 1.1. It is evident from table 1.1 that bulk density is found to be decreasing with increase in Al-Cr content x.

The particle size of the Al-Cr substituted nickel ferrite powders was calculated by using the most intense peak (311) and using the Debye-Scherer's relation for small and uniform sized cubic crystals mentioned below [28].

$$t = \frac{0.9\lambda}{\beta \cos\theta} \qquad (4)$$

where, λ is wavelength of the Cu-Kα radiation, β is the full width at half maximum θ is Bragg's angle.

The obtained values of the crystallite size are presented in Table 1.1. It is observed that particle size decreases with increasing Al-Cr content *x*.

Morphological Analysis

3.2 Scanning electron microscopy (SEM)

Morphology of the prepared samples was studied using scanning electron microscope (SEM). Fig. 1.2 represents the scanning electron micrographs for $NiAl_{2x}Cr_xFe_{2-3x}O_4$ (where, x = 0.0, 0.1) system. Scanning electron micrographs indicates the formation of nano-sized grains of the $NiAl_{2x}Cr_xFe_{2-3x}O_4$ ferrite powder. The average grain size was determined from SEM image by linear intercept method estimated using the relation [29].

$$D = 1.5\ L / M.\ N \qquad (5)$$

where, L is a total test line length, M is magnification, N is total number of the samples.

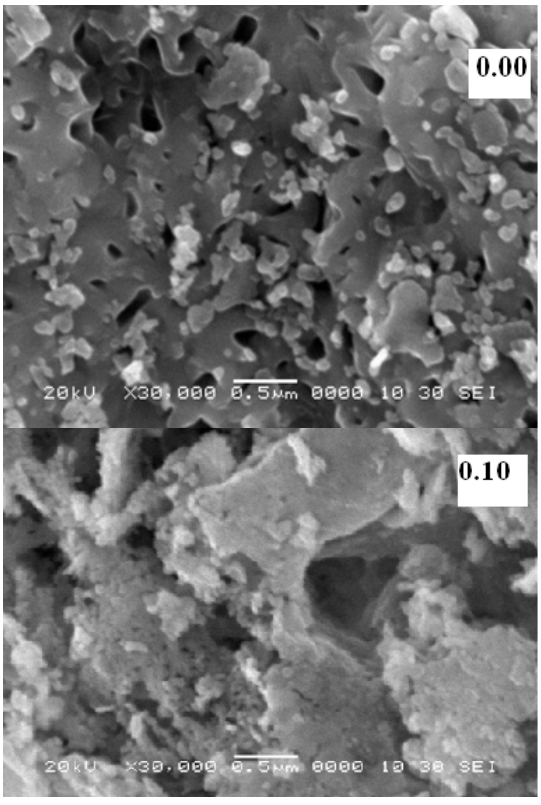

Fig. 1.2 Typical SEM images of $NiAl_{2x}Cr_xFe_{2-3x}O_4$ nanoparticles for (x = 0.0 and 0.1)

Table 1.2 Average grain size (G), Specific surface area (S) and elemental percentage (EDAX) of $NiAl_{2x}Cr_xFe_{2-3x}O_4$ nanoparticles

x	G (nm)	S (m^2/g)	Ni^{2+} (%)	Al^{3+} (%)	Cr^{3+} (%)	Fe^{3+} (%)	O^{2-} (%)
0.0	87	12.72	5.87	87.52	-	-	6.61
0.1	83	13.65	7.21	80.65	2.03	2.06	8.05
0.2	76	15.25	6.24	78.66	3.35	3.92	7.83

The average grain size is found to be in nanometer range and of the order of 69-87 nm, which confirming the nanocrystalline nature of the prepared samples. From the SEM micrographs it is seen that the ferrite powder is an aggregation of particles. The particles observed as uniform grains confirm the crystalline nature of the ferrites. The specific surface area of all the samples using SEM images was calculated according to the relation [30].

The values of average grain size and specific surface area are given in Table 1. 2. The large value of specific surface area indicates the nanocrystalline nature of all the samples under investigation. The decrease in average grain size increases the specific surface area.

Compositional Analysis

3.3 Energy dispersive X-ray analysis (EDAX)

The elemental analysis was carried out by using energy dispersive X-ray spectrometer. The typical EDAX pattern of $NiAl_{2x}Cr_xFe_{2-3x}O_4$ nanoparticles (x = 0.0) is shown in Fig 1.3. The EDAX pattern of the sample $NiAl_{2x}Cr_xFe_{2-3x}O_4$ (x = 0.0) provides the information about the elemental and atomic composition in the sample.

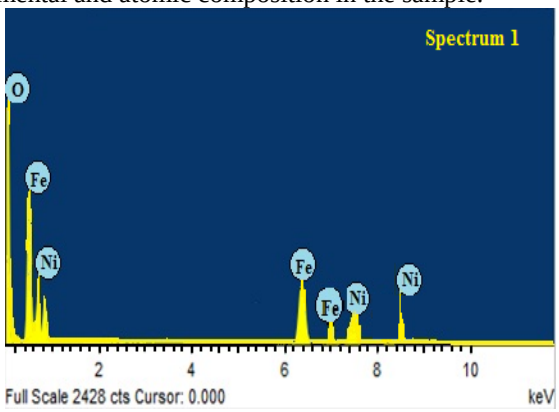

Fig. 1.3 Typical EDAX patterns of $NiAl_{2x}Cr_xFe_{2-3x}O_4$ nanoparticles for (x = 0.0)

The results of EDAX clearly show that $NiAl_{2x}Cr_xFe_{2-3x}O_4$ contain Ni^{2+}, O^{2-} and Fe^{3+} ions without any impurity. EDAX results showed sample to be homogeneous with the expected Ni: Fe: O: ratios.

The EDAX results of the present samples confirm that the precursor used for the synthesis have fully undergone the chemical reaction to form the single phase $NiAl_{2x}Cr_xFe_{2-3x}O_4$ system in nanocrystalline form. Table 1.2 gives elemental percentage for $NiAl_{2x}Cr_xFe_{2-3x}O_4$ system. It is evident from table 1.2 that the elements Ni^{2+}, O^{2-} and Fe^{3+} ions are found to be in stoichiometric proportions.

3.4 Fourier transforms infrared spectroscopy

Fourier transforms infrared spectra of the $NiAl_{2x}Cr_xFe_{2-3x}O_4$ **(**x = 0.0, 0.1 and 0.2) system samples recorded at room temperature are shown in Fig. 1.4. The FTIR spectra show the two principle absorption bands in the range of 300 cm^{-1} to 800 cm^{-1}, the first absorption band is seen at around 396.09 cm^{-1} and second band is around 600 cm^{-1}. The absorption bands (ν_1 and ν_2) correspond to intrinsic lattice vibrations of octahedral and tetrahedral coordination compounds in the spinel structure respectively. The difference in frequency between the characteristic vibrations ν_1 and ν_2 may be attributed to the long bond length of oxygen-metal ions in the tetrahedral sites. The behaviour of ν_1 and ν_2 vibrations mainly depends on the identification of transition metal ions in the tetrahedral site and to a smaller extent on the ions situated at the octahedral sites. There is no trend has been observed in frequency band position with addition of Al-Cr ions. Similar FTIR spectra have been reported in literature for ceramically prepared Cr substituted ferrite system [31]. These slight deviations in the positions of peaks are mainly due to the factors like method of preparation, grain size and density [32, 33]. The force constant can be calculated for tetrahedral site (K_t) and octahedral site (K_o) by using the method suggested by Waldron [34, 35]:

$$K_t = 7.62 \times M_A \times \upsilon_1^2 \times 10^{-7} \text{ N/m} \quad (6)$$

$$K_0 = 10.62 \times (M_B/2) \times \upsilon_2^2 \times 10^{-7} \text{ N/m} \quad (7)$$

where, M_A and M_B are the molecular weights of cations at A and B-sites, respectively. The values of ν_1 and ν_2 and K_t and K_0 are given in Table 1.3. It is observed from table that K_t and K_0 both vary as per the variation in ν_1 and ν_2 values. The bond length corresponding to tetrahedral (A) and octahedral [B] sites was calculated and their values are listed in Table 1.3.

The force constant is second derivative of potential energy with respect to the site radius, while the other independent parameters are kept constant. According to Waldron the force constant K_t and K_0 for respective sites are given by where, M_1 and M_2 are molecular weight of cations on A and B sites, respectively.

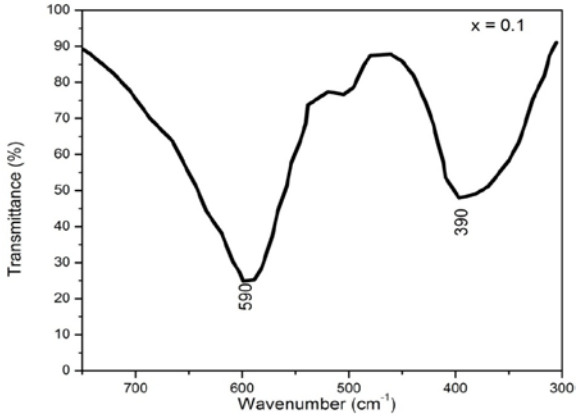

Fig. 1.4: Typical FTIR pattern of $NiAl_{2x}Cr_xFe_{2-3x}O_4$ nanoparticles for (x = 0.1)

Table 1.3 Infrared absorption frequency bands position (ν_1) and (ν_2), force constant (Kt and K_0) and bond length of tetrahedral (R_A) and octahedral site (R_B) of $NiAl_{2x}Cr_xFe_{2-3x}O_4$ nanoparticles

x	ν_1 cm^{-1}	ν_2 cm^{-1}	K_t x10^5 dyne/cm	K_0 x 10^5 dyne/cm	R_A (Å)	R_B (Å)
0.0	599	399	1.074	1.543	1.945	0.2450
0.1	590	390	1.062	1.527	1.932	0.2445
0.2	599	396	1.076	1.572	1.928	0.2443

The bond length R_A and R_B have been calculated using the formula given by Gorter [36, 37]. In the present system it is observed that no systematic variation in force constant was observed with the increase in Al- Cr content 'x'.

4. Conclusions

The nanocrystalline $NiAl_{2x}Cr_xFe_{2-3x}O_4$ of different compositions with x = 0.0, 0.1, 0.2 were successfully synthesized by a sol-gel auto combustion method. XRD results confirm the prepared samples are in the nano-scale region having a cubic spinel structure with single phase. Lattice parameters, X-ray density, bulk density and particle size decrease with the increase in Al-Cr content x. The crystallite size confirms the nanocrystalline nature of the samples. The average grain size obtained from scanning electron microscopy was found in the range of 76-87 nm. Energy dispersive spectroscopy analysis confirmed that the synthesized samples were near stoichiometric. Infrared spectra exhibit two distinct absorption bands near about 400 cm^{-1}, 600 cm^{-1} and octahedral and tetrahedral sites, respectively indicating the characteristic features spinel ferrites.

References

[1] D.S. Mathew, R.-S. Juang, Chemical Engineering Journal, 129 (2007) 51-65.
[2] M. Ajmal, A. Maqsood, Journal of Alloys and Compounds, 460 (2008) 54-59.
[3] A.A. Hossain, S. Mahmud, M. Seki, T. Kawai, H. Tabata, Journal of Magnetism and Magnetic Materials, 312 (2007) 210-219.
[4] K.K. Bharathi, G. Markandeyulu, C. Ramana, The Journal of Physical Chemistry C, 115 (2010) 554-560.
[5] S. Sun, H. Zeng, D.B. Robinson, S. Raoux, P.M. Rice, S.X. Wang, G. Li, Journal of the American Chemical Society, 126 (2004) 273-279.
[6] A.M. Wahba, M.B. Mohamed, Ceramics International, 40 (2014) 6127-6135.
[7] G. Busca, V. Lorenzelli, G. Ramis, R.J. Willey, Langmuir, 9 (1993) 1492-1499.
[8] A.E. Job, F.S. Bellucci, F.C. Cabrera, A.F. DE Siqueira, E.R. Budemberg, L.O. Salmazo, Natural Rubber Materials: Volume 2: Composites and Nanocomposites, 8 (2013) 432.
[9] V.G. Harris, A. Geiler, Y. Chen, S.D. Yoon, M. Wu, A. Yang, Z. Chen, P. He, P.V. Parimi, X. Zuo, Journal of Magnetism and Magnetic Materials, 321 (2009) 2035-2047.
[10] J. Liu, L. Wang, F. Li, Journal of materials science, 40 (2005) 2573-2575.
[11] A. Ceylan, Core/shell structured magnetic nanoparticles synthesized by inert gas condensation, ProQuest, 2007.
[12] M.P. Pileni, Advanced Functional Materials, 11 (2001) 323-336.
[13] A. Chatterjee, D. Das, S. Pradhan, D. Chakravorty, Journal of magnetism and magnetic materials, 127 (1993) 214-218.
[14] C. Lin, W. Böttcher, M. Chou, C. Creutz, N. Sutin, Journal of the American Chemical Society, 98 (1976) 6536-6544.
[15] S.-H. Byeon, K. Park, M. Itoh, Journal of Solid State Chemistry, 121 (1996) 430-436.
[16] N.R. Jana, Y. Chen, X. Peng, Chemistry of materials, 16 (2004) 3931-3935.
[17] F. Magalhães, M. Pereira, S. Botrel, J. Fabris, W. Macedo, R. Mendonca, R. Lago, L. Oliveira, Applied Catalysis A: General, 332 (2007) 115-123.
[18] A. Ghatage, S. Patil, S.K. Paranjpe, Solid state communications, 98 (1996) 885-888.
[19] S. Patange, S.E. Shirsath, K. Lohar, S. Jadhav, N. Kulkarni, K. Jadhav, Physica B: Condensed Matter, 406 (2011) 663-668.
[20] A. Raghavender, D. Pajic, K. Zadro, T. Milekovic, P.V. Rao, K. Jadhav, D. Ravinder, Journal of Magnetism and Magnetic Materials, 316 (2007) 1-7.
[21] I. Ismailzade, G. Smolenskii, V. Nesterenko, F. Agaev, physica status solidi (a), 5 (1971) 83-89.

[22] H. Kavas, N. Kasapoğlu, A. Baykal, Y. Köseoğlu, chemical papers, 63 (2009) 450-455.
[23] R. Fleming, F. DiSalvo, R. Cava, J. Waszczak, Physical Review B, 24 (1981) 2850.
[24] H.S.C. O'Neill, A. Navrotsky, American Mineralogist, 68 (1983) 181-194.
[25] S. More, R. Kadam, A. Kadam, A. Shite, D. Mane, K. Jadhav, Journal of Alloys and Compounds, 502 (2010) 477-479.
[26] W.D. Callister, D.G. Rethwisch, Materials science and engineering: an introduction, Wiley New York, 2007.
[27] P. Coppens, X-ray charge densities and chemical bonding, International Union of Crystallography, 1997.
[28] M. Irfan, U. Khan, W. Li, W. Kong, K. Javed, X. Han, Journal of Alloys and Compounds, 691 (2017) 1-7.
[29] X.-H. Wang, R.-Z. Chen, Z.-L. Gui, L.-T. Li, Materials Science and Engineering: B, 99 (2003) 199-202.
[30] A. Peigney, C. Laurent, E. Flahaut, R. Bacsa, A. Rousset, Carbon, 39 (2001) 507-514.
[31] A. Rosencwaig, Canadian Journal of Physics, 48 (1970) 2857-2867.
[32] S.E. Shirsath, B. Toksha, R. Kadam, S. Patange, D. Mane, G.S. Jangam, A. Ghasemi, Journal of Physics and Chemistry of Solids, 71 (2010) 1669-1675.
[33] A. Czímerová, J. Bujdák, R. Dohrmann, Applied Clay Science, 34 (2006) 2-13.
[34] P. Hankare, R. Patil, U. Sankpal, S. Jadhav, P. Lokhande, K. Jadhav, R. Sasikala, Journal of Solid State Chemistry, 182 (2009) 3217-3221.
[35] W. White, B. DeAngelis, Spectrochimica Acta Part A: Molecular Spectroscopy, 23 (1967) 985-995.
[36] V. Kawade, G. Bichile, K. Jadhav, Materials Letters, 42 (2000) 33-37.
[37] A. Birajdar, S.E. Shirsath, R. Kadam, M. Mane, D. Mane, A. Shitre, Journal of Applied Physics, 112 (2012) 053908.